THE JOURNAL OF PHYSICAL CHEMISTRY C

Article

Interplay Between Hydrogen Bonding and Molecule-Substrate Interactions in the Case of Terephthalic-Acid Molecules on Cu(001) Surfaces.

Javier Daniel Fuhr, Alvaro Carrera, Natalia Murillo-Quirós, Lucila Cristina, Albano Cossaro, Alberto Verdini, Luca Floreano, Julio Esteban Gayone, and Hugo Ascolani

J. Phys. Chem. C, **Just Accepted Manuscript** • DOI: 10.1021/jp305455v • Publication Date (Web): 27 Dec 2012

Interplay between Hydrogen Bonding and Molecule-Substrate Interactions in the Case of Terephthalic-Acid Molecules on Cu(001) Surfaces.

J. D. Fuhr,[*,†] A. Carrera,[†] N. Murillo-Quirós,[†] L. Cristina,[†] A. Cossaro,[‡] A. Verdini,[‡] L. Floreano,[‡] J. E. Gayone,[†] and H. Ascolani[*,†]

Centro Atómico Bariloche, CNEA, and CONICET, Av. E. Bustillo 9500, R8402AGP, Bariloche, Argentina., and CNR-IOM, Laboratorio TASC, Basovizza SS14 Km. 163.5, I-34149 Trieste, Italy,

E-mail: fuhr@cab.cnea.gov.ar; ascolani@cab.cnea.gov.ar

KEYWORDS: terephthalic acid, Cu(001),self-assembling,DFT, scanning-tunneling microscopy,X-ray photoelectron spectroscopy

[*]To whom correspondence should be addressed
[†]Centro Atómico Bariloche
[‡]Elettra

Abstract

The adsorption and self-assembling properties of terephthalic acid (TPA) molecules deposited on Cu(001) at room temperature have been systematically studied using both experimental and theoretical tools. The system forms two phases at room temperature, the metastable β-phase and the stable 3×3 one. In the case of the β phase, the low-energy electron diffraction and scanning-tunneling microscopy (STM) results indicate that the β phase has a $(9\sqrt{2} \times 2\sqrt{2})$R45° unit cell with exactly the same molecular coverage as the 3×3 phase. In addition, the high-resolution X-ray photoelectron spectroscopy O1s spectra indicate that the irreversible $\beta \rightarrow 3 \times 3$ transition involves the following two processes: i) deprotonation of the complete carboxyl groups remaining in the metastable phase and ii) re-arrangement of the molecules into the 3×3 configuration. On the other hand, we explored possible molecular configurations for the β phase with different degree of deprotonation (including structures with Cu adatoms) by means of density functional theory calculations. Our theoretical results indicate the formation of strong bonds between the O atoms in carboxylates and the Cu atoms of the surface, which causes a bending of the molecules and a buckling of the first Cu layer. In the 3×3 phases, we show that the bending produces observable effects in the molecular STM images. We also observed that the strong interaction between the carboxylates and the Cu atoms at the step edges drives the reorientation of the surface steps along the $< 100 >$ crystallographic directions.

Introduction

Engineering of supramolecular structures grown by spontaneous self-assembling on metallic surfaces is important in nanotechnology.[1] Molecules with well-defined shapes and multiple sites that engage in strong directional interactions are now widely used to build new ordered materials on surfaces.[2,3] In this article we consider the ordered phases formed by terephthalic acid (TPA) molecules on Cu(001) surfaces at room temperature (RT) as a model system to investigate the subtle energetical balance between molecule-substrate interactions and intermolecular interactions. A

deep understanding of this balance is important to predict the physical-chemical properties of 2D supramolecular structures grown in surfaces.[4]

TPA is the simplest case of rod-like polybenzene dicarboxylic acids, a family of molecules which has been widely used as linkers to build interesting 2D supramolecular structures.[5] The versatility of these molecules is strongly related to the carboxyl groups (RCOOH). It is well established that the RCOOH group usually remains intact upon adsorption on low-reactivity surfaces, such as Au(111)[6,7] and graphite HOPG[8] surfaces. The group can lose the proton when deposited on more reactive substrates like, for example, Cu[9–14] or Ag[15,16] surfaces. In the first case, the neutral TPA molecules form highly-ordered supramolecular structures governed by strong [O-H$\cdots$ O] hydrogen bonds.[6] In the second case, deprotonation of carboxyl groups opens the route to metal-organic complexes offering a variety of possibilities to produce 2D magnetic networks based on Fe[17–21] and Mn[22] with exciting properties.

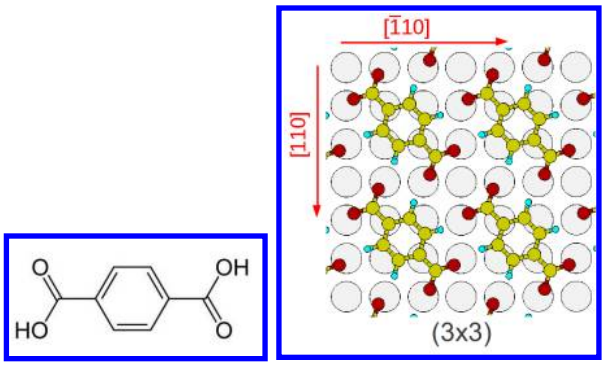

Figure 1: Left: Scheme of the TPA molecule. Right: Structural model for the (3×3) phase of deprotonated TPA molecules on Cu(001). The yellow, light-blue and red circles represent the C, H and O atoms of the deprotonated TPA molecules, respectively. Large open circles represent the Cu atoms of the top surface layer.

Although the TPA/Cu(001) system has been widely applied to grow 2D supramolecular structures, there are important issues concerning the pure system which are still open. The phases formed by TPA molecules on the Cu(001) surface have been previously investigated by Stepanow et al.[12] by means of scanning-tunneling microscopy (STM), X-ray photoelectron spectroscopy (XPS), and near-edge X-ray absorption fine structure (NEXAFS). Three distinct ordered phases evolving with increasing temperature were observed. Deposition on samples kept at temperatures

below 230K produced the α phase which, according to the reported STM image, consists of thin and long molecular ribbons oriented along specific directions of the substrate. Both the anisotropic growth of the islands as well as the C 1s and O 1s XPS spectra taken on this phase are consistent with neutral TPA molecules interacting through [O-H$\cdots$ O] hydrogen bonds. Increasing the sample temperature to about 273 K produced the transformation of the low-temperature phase into a metastable ordered phase called β. It was speculated that this phase contains both complete and deprotonated carboxyl groups in equal amounts. At RT, a mixture of the β and γ phases was observed. The γ phase has a 3×3 periodicity and is composed by TPA molecules with the two carboxyl groups deprotonated (terephthalates).[23] Finally, a pure 3×3 phase was obtained after a mild annealing of the sample to 400K.

Figure 1 shows a scheme of the structural model proposed for (3×3) phase. The O atoms are expected to form strong Cu-O bonds and also weak hydrogen bonds with the H atoms of the benzene ring. It is now well recognized that [C-H$\cdots$ O] hydrogen bonds play a fundamental role in determining the packing of organic molecules in the solid state.[24] Similarly, [C-H$\cdots$ O] hydrogen bonds are expected to be an important factor for the stabilization of two-dimensional molecular structures on surfaces. In the particular case of the 3×3 structure, the formation of [C-H$\cdots$ O] bonds (eight bonds per molecule) has been regarded as the main driving force for the formation of the phase.[12] However, Ge et al.[23] did not observe any evidence for this type of H bonding in their high-resolution electron energy-loss spectroscopy (HREELS) spectra and, hence, suggested that TPA islanding may be due to surface-mediated attractive interactions.[4] As the atomic structure of the (3×3) has not been quantitatively investigated neither experimentally nor theoretically, the relative importance of these effects is not known.

The β phase is also interesting from the structural point of view since, in addition to the weak [C-H$\cdots$ O] bonds found in the 3x3 phase, it would involve strong [O-H$\cdots$ O] bonds. However, there is almost no quantitative information on this metastable phase in the literature so far. A quantitative knowledge of the structure would help to gain more understanding on the deprotonation process of the TPA molecules on the Cu(001) surface.

In this work we performed a systematic and quantitative characterization of the atomic and electronic structures of the 3×3 and β phases by combining different experimental techniques, namely, LEED, STM, and high-resolution XPS (HR-XPS), with van-der-Waals DFT calculations. Our results allowed us to perform a detailed analysis of the competition between substrate/molecule interactions and hydrogen-bond interactions taking place in the TPA/Cu(001) system.

Methods

Experimental details

Two independent ultra-high vacuum systems were used to perform the experiments involved in this work. The LEED and STM experiments were carried out at Bariloche using an ultra-high vacuum system from Omicron-Nanotechnology. The HR-XPS experiments were carried out at the ALOISA beam line[25,26] of the ELETTRA synchrotron, at Trieste.

The base pressures in both chambers were in the low 10^{-10} mbar range. The Cu(001) surfaces were prepared by doing cycles of sputtering with Ar at 1.5 KeV and annealing at 770K. The TPA molecules (Sigma-Aldrich, 98% purity) were used as received. In all cases analyzed in this work the TPA/Cu(001) samples were prepared by dosing TPA molecules (submonolayer range) on the substrate at RT. The molecules were evaporated from a resistivity heated BN crucible at a rate of about 0.1 monolayer (ML) per minute. We define 1 ML as the surface coverage corresponding to the 3×3 phase, i.e. a molecular coverage of 1 TPA molecule per 9 Cu atoms in the top surface layer. In ALOISA we checked the formation of the 3×3 phase as well as the quality of the clean Cu(001) surface by Reflection High-Energy Electron Diffraction (RHEED).

All the reported STM images were taken at RT (unless otherwise stated) using W tips. Negative sample bias voltages correspond to occupied-state images. The thermal drift was compensated during the measurements by applying the facility provided by the MATRIX software used to control the STM.

The HR-XPS data were obtained using a p-polarized X-ray beam at grazing incidence (about

4°). The spectra, taken with a photon energy of 655 eV, were measured in normal emission by means of a hemispherical electron analyzer with angular acceptance of 2° and an overall energy resolution of 300 meV. Four energy windows centered on the regions of the Fermi edge and the Cu 3p, C 1s and O 1s core levels, were typically acquired by means of a 2D delay-line detector.[27]

Theoretical details

The DFT calculations were performed using the Quantum-ESPRESSO package,[28] which is an implementation of the plane-wave with ultrasoft-pseudopotentials approach. The exchange-correlation effects were treated using the second version of van der Waals density functional (vdW-DF)[29] with improved exchange.[30] For the surface calculations we have used the slab method, with four Cu layers representing the surface and an equivalent vacuum size of seven layers. For all the calculations, we fixed the two lower layers while all other atoms are allowed to relax. We used a wave-function/charge cutoff of 30/300 Ry, and Brillouin integrations were done using a grid of $15 \times 15 \times 1$, $5 \times 5 \times 1$ and $3 \times 3 \times 1$ k-points for the unit cell, the 3×3 supercell and the 5×5 supercell respectively.

For a given configuration corresponding to N molecules adsorbed on the surface, the mean adsorption energy per molecule is calculated by

$$E_{\mathrm{ads}}(\mathrm{TPA}) = -\left[\frac{E_{\mathrm{total}} - E_{\mathrm{surface}} - N_{\mathrm{H}} E_{\mathrm{ads}}(\mathrm{H})}{N} - E_{\mathrm{TPA}}\right] \quad (1)$$

where: E_{total} is the total energy of the system with the adsorbed molecules; E_{surface} is the total energy of a clean surface with the same area; N_{H} is the number of dissociated H atoms, with $E_{\mathrm{ads}}(\mathrm{H}) = 0.18$ eV its corresponding adsorption energy on the Cu(001) surface; and E_{TPA} is the total energy of an isolated TPA molecule.

In all the calculations we have applied the dipole correction, that takes into account the possible dipoles that can appear on the surfaces.[31] As the two surfaces of the slab are not equal, the lower one clean while the upper one with adsorbed molecules, the difference in the surfaces dipoles is

compensated in the middle of the vacuum by an artificial jump in the potential. The simulated STM images were calculated within the Tersoff-Hamann approximation.[32]

Results

Experimental Results

LEED.

Figures 2(a) and 2(b) show two LEED patterns measured with 37 and 51 eV, respectively, which are representative of freshly prepared TPA/Cu(001) surfaces. These patterns, which have not been previously reported in the literature, were observed to be highly unstable under the effect of the primary electron beam of the LEED. The effect is illustrated by the series of patterns in Figures 2(a), 2(c), and 2(d). As seen in these figures, the initial LEED pattern completely transform into a (3×3) one within a period of time of 30 minutes. We note, however, that this effect is not observed when the e-beam is turned off; in this case the lifetime of the initial pattern was observed to be several hours. It should be noted that the initial pattern in Figure 2(a) also contains weak 3×3 spots.

In Ref. 12, it was shown that deposition of TPA on Cu(001) at RT produces a surface where the (3×3) phase coexists with the metastable β one. Therefore, the LEED patterns shown in Figures 2(a) and 2(b) should correspond to a mixture of these phases. What it is unexpected, however, is the fact that the pattern of the metastable β phase systematically turned out to be highly dominant in fresh samples.

From a detailed analysis of the patterns in Figures 2(a) and 2(b), we concluded that they correspond to a $(9\sqrt{2} \times 2\sqrt{2})R45^\circ$ superstructure ($9\sqrt{2}$ from hereafter). This fact can be corroborated by comparing the experimental patterns with the simulated one in Fig. 2(e). The spots which can not be explained by the $9\sqrt{2}$ superstructure correspond to the (3×3) phase.

STM. Figure 3(a) shows an STM image with molecular resolution where two inequivalent rotated domains of the β phase can be clearly seen. The image was taken on a fresh sample

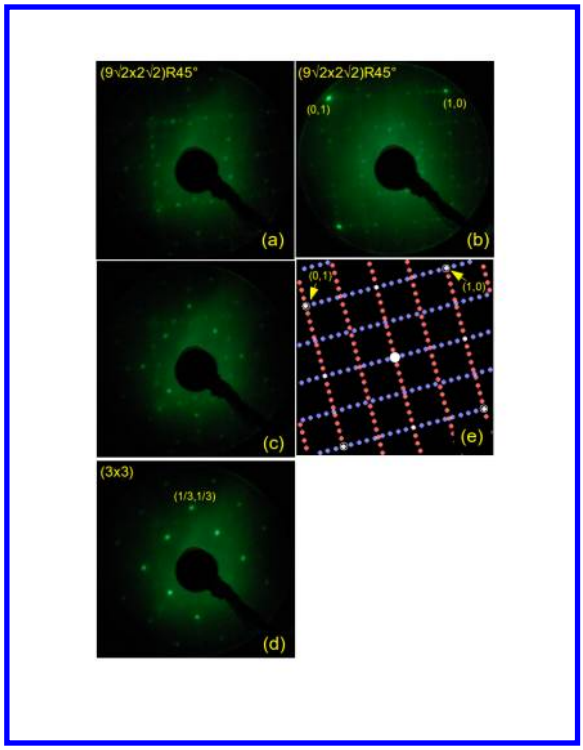

Figure 2: Panels (a) and (b): Experimental LEED patterns representative of fresh TPA/Cu(001) surfaces prepared at RT; the corresponding electron energies are 37 and 51 eV, respectively. The (1×1) spots are outside the screen in pattern (a) while they are clearly visible in pattern (b). Patterns (c) and (d) show the transformation of the pattern (a) into a 3×3 one; they were recorded after 9 and 30 minutes, respectively, of having measured the initial pattern. The observed phase transition is induced by the primary electron beam of the LEED (see text for details). Panel (e): simulated LEED pattern[33] for a $(9\sqrt{2} \times 2\sqrt{2})R45^\circ$ unit cell; the blue and red spots correspond to the patterns of the two inequivalent domains of the superstructure.

where no further bombarding with the LEED electron beam was done. Remarkably, this area of the surface was scanned along several hours at RT and we did not detect any transformation to the 3×3 one. In agreement with the LEED results, the STM experiments show that the β phase covers most of the surface, even when it was always found coexisting with 3×3 islands.

In order to determine the unit cell of the β phase we used STM images where domains of the (3×3) phase are also seen. These kind of images allowed us to perform a precise correction of the remaining distortions of the images, since we could take the (3×3) superstructrure as a reference. We determined that the unit cell of the β phase is rectangular ($\alpha = 90^\circ \pm 1^\circ$) with sides of 7.3 ± 0.5 Å and 34 ± 2 Å . These values agree very well with the corresponding exact values of the $9\sqrt{2}$ unit cell (7.22 Å and 32.50 Å) giving support to the conclusions derived from the LEED experiments. We note that neither the STM images nor the LEED pattern of the β phase are consistent with the $\begin{pmatrix} 2 & -2 \\ 4 & 5 \end{pmatrix}$ unit cell proposed by Stepanow et al.[12] Finally, as we shall show in the next section (see Figure 11), there are four molecules in the unit cell and, therefore, the coverage of the phase is 1 TPA molecule per 9 Cu atoms of the first substrate layer. Notably, the $9\sqrt{2}$ phase has exactly the same molecular coverage as the 3×3 phase (from this point we will refer to "β phase" as " $9\sqrt{2}$ phase")

The STM image of Figure 3 (a) also illustrates about another interesting effect systematically observed in our images: the straightening of monoatomic surface steps along the $< 100 >$ crystallographic directions induced by the adsorption of the TPA molecules for submonolayer coverages. This is contrast to the fact that for Cu(001) surfaces the energetically more stable steps are those aligned along $< 110 >$ directions. We note that a similar effect was observed for submonolayer coverage of tetrafluoro-tetracyanoquinodimethane (F-TCNQ) adsorbed on Cu(001) surfaces.[34] The re-orientation effect is illustrated with more detail in Figure 3 (b), which was measured after cooling the sample to 200K in order to reduce the mobility of the molecules. This image shows a small monoatomic terrace with the square-like-shape close to an island of molecules in the $9\sqrt{2}$ phase. The monoatomic steps are decorated at the lower edge by a few lines of molecules arranged with a similar orientation as that observed in the $9\sqrt{2}$ island, indicating that the interaction of the

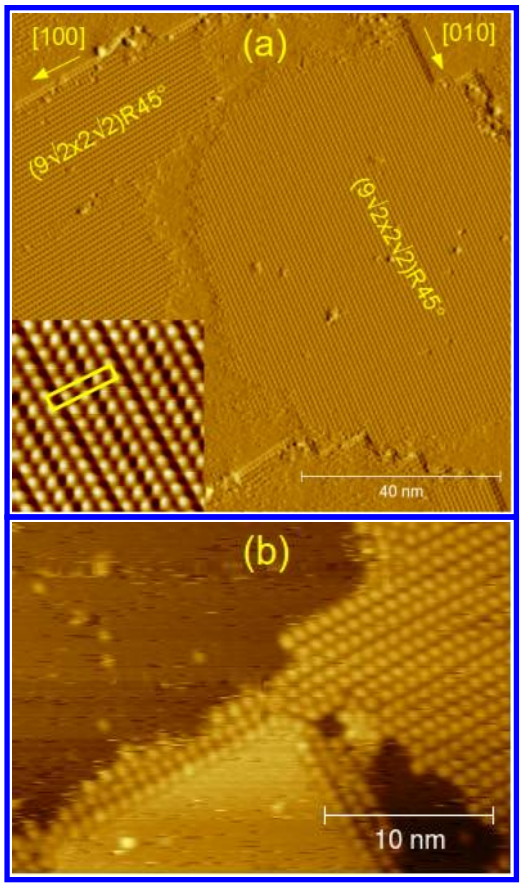

Figure 3: (a): Occupied-state STM image (gradient mode) where two 90° rotated domains of the $9\sqrt{2}$ phase are seen. Tunneling conditions: -2V/10pA. The inset shows a zoomed area (100x100 Å^2) of the domain on the right; a yellow rectangle is superimposed to the image indicating the unit cell of the superstructure. (b): STM image taken with the same tunneling conditions as in (a) but with the sample cooled to around 200K.

TPA molecules with the Cu atoms at the steps is responsible for this effect. These observations would be related to the origin of the multi-step squared-shape terraces recently reported by Tait et.al. for a saturated monolayer of TPA on Cu(001).[35]

In addition, Figure 4 shows a TPA/Cu(001) surface after annealing the sample to 400K for a few minutes. The resulting surface is composed of monoatomic squared-shape terraces with their delimiting steps aligned along the $< 100 >$ crystallographic directions of the substrate; the average size of the terraces is around 300×300 Å^2. Islands of the 3×3 phase cover the upper surface of the square terraces. Also, it can be seen in this image that the straight segments of the steps are decorated by molecules. We therefore conclude that the typical annealing used to obtain the 3×3

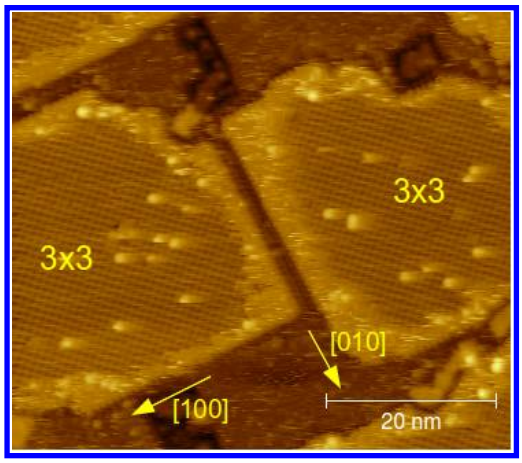

Figure 4: Occupied-state STM image of the TPA/Cu(001) surface after annealing the sample to 400K. Tunneling conditions: -2V/10pA.

phase in fact produces a surface with a high-density of surface steps oriented along the $< 100 >$ crystallographic directions. The observed drastic change of the surface morphology with annealing at 400K is probably related to the thermal dependence of the diffusion of the Cu atoms at the steps, which is a thermally activated process. Kinks are known to reach a high mobility at 360 K in Cu(001) surfaces.[36]

XPS. As discussed above, the $9\sqrt{2}$ phase covers most of the surface when submonolayer amounts of TPA molecules are adsorbed on Cu(001) at RT. This situation was observed to be stable for a few hours, provided the surface were not irradiated with the primary electron gun of the LEED. These properties of the $9\sqrt{2}$ phase allowed us to characterize it by means of HR-XPS. Figure 5 shows the O 1s XPS spectrum obtained after adsorbing the TPA at RT (lower one), together with 3 spectra measured after annealing the prepared sample during 5 minutes at different temperatures. The four spectra were normalized to the intensity of the corresponding Cu 3p peak and, therefore, their relative intensities are comparable. To calibrate the binding energy of each spectrum we considered both the Fermi level edge and the Cu 3p peak.

Therefore, the lower spectrum in Fig. 5 is representative of the $9\sqrt{2}$ phase. The upper spectrum, in turn, corresponds to the 3×3 phase of the system, as checked by RHEED. The spectrum of the $9\sqrt{2}$ phase presents, apart from the prominent peak centered around 531 eV that corresponds to

carboxylates, a clear shoulder towards higher binding energies (which extends up to about 534 eV) which strongly suggests the existence of complete carboxyl groups, as proposed by Stepanow et al.[12]

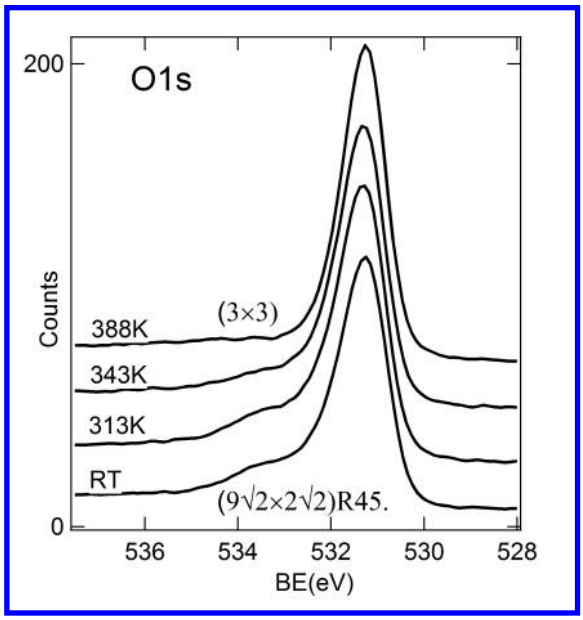

Figure 5: Series of O1s spectra of a submonolayer amount of TPA adsorbed on Cu(001) at RT as a function of the annealing temperature of the prepared sample. The lower and upper spectra are representative of the $9\sqrt{2}$ and 3×3 phases, respectively.

In Figure 6 we shows a component analysis of the O 1s spectrum representative of the $9\sqrt{2}$ phase. We used three Voigt functions and a Shirley-type background to fit the experimental spectrum. The optimized parameter values obtained for components I, II and III are the following. Gaussian widths: 0.86 , 1.3, and 1.4 eV respectively; the three lorentzian widths were fixed to 0.25 eV. Binding energies: 531.1, 531.7, and 533.3 eV, respectively. Finally, the resulting relative peak areas for the components I, II and III turned out to be 56%, 31% and 13%, respectively.

The binding-energy values obtained for components I and III agree very well with the previously-reported values for O atoms in carboxylates bonded to Cu surfaces and for the OH part of the RCOOH groups, respectively.[9,12–14,19,37] Thus, component III confirms that the $9\sqrt{2}$ phase comprises carboxyl groups. Regarding component II, we note that it is shifted by 1.6 eV from component III. We recall that the shift between the O 1s peaks corresponding to OH and C=O groups is 1.4 eV for TPA molecules in bulk and 2.05 eV for TPA in gas phase.[38,39] Thus, component II

should contain the contribution of the C=O groups although, however, it could also include the contributions of other chemically-inequivalent O atoms of the $9\sqrt{2}$ structure, as suggested by the simulated O1s spectrum shown in the inset. We shall discuss the simulated spectrum in the next section.

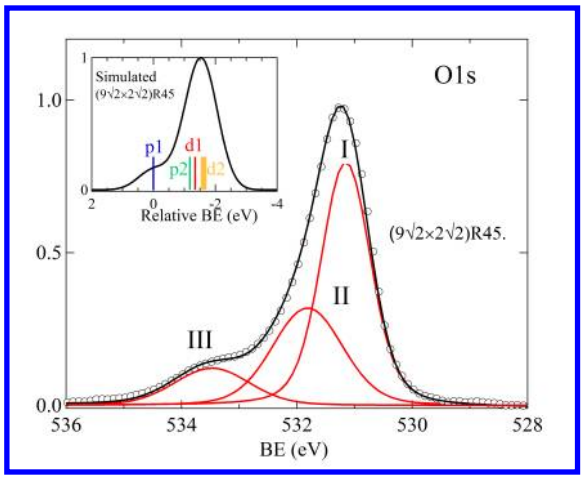

Figure 6: Analysis of the O1s spectra corresponding to the $9\sqrt{2}$ phase. Experimental data: open circles; result of the fitting: continuous black line. The two spectra are normalized to their corresponding maximum. Inset: simulated spectra as explained in the text.

The O 1s spectra in Figure 5 show the irreversible transition from the partially-protonated $9\sqrt{2}$ phase to the fully-deprotonated 3×3 induced by temperature. Notice that annealing the sample to 313K does not produce any noticeable change on the O 1s peak while, in turn, the annealing to 343K produces a clear reduction of the shoulder and, at the same time, an increment of the main-peak intensity. Notably, a quantitative analysis of the spectra indicates that the total area under the normalized O 1s spectra remains constant during the transition, as expected for a transition between two phases with the same molecular coverage. We therefore conclude that the transition involves the following two processes: i) the deprotonation of the carboxyl groups remaining in the $9\sqrt{2}$ phase and ii) the eventual re-arrangement of the molecules into the 3×3 configuration.

DFT calculations

In order to gain more understanding on the physical-chemical processes taking place at the molecule/substrate interfaces formed by this system we carried out a thorough theoretical study of the adsorption of

the TPA molecules on the Cu(001) surface.

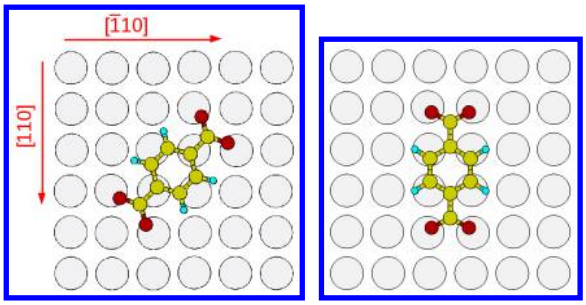

Figure 7: Two adsorption geometries for isolated deprotonated TPA molecules on Cu(001) from DFT calculations. Left: molecule oriented in the [100] direction. Right: molecule oriented in the [110] direction.

We first studied a single TPA molecule in a 5×5 supercell which corresponds to the system with the lowest molecule-molecule interaction of our calculations. We considered both neutral molecules and molecules with the two carboxyl groups deprotonated (also called totally-deprotonated TPA molecules in this article), and in both cases we found two local minimum energy configurations with the center of the benzene in a hollow site and the molecule oriented in [100] and [110] surface directions (see Fig. 7). In both cases, neutral and deprotonated molecule, the minimum energy corresponds to the molecule aligned in the [100] direction (Fig. 7, left panel) with adsorption energies of 1.80 eV and 2.08 eV, respectively. The gain in energy by dissociation of the molecule, with the H remaining on the surface (see Eq. (1)), is then 0.28 eV. On the other hand, the configurations with the molecule aligned in the [110] direction have lower adsorption energies by 0.20 eV.

Notably, our calculations indicate that the molecule/substrate interaction is strong in both neutral and deprotonated molecule. In the lowest-energy configuration, the deprotonated molecule is bent with a difference of 0.26 Å between the height of the benzene ring and the O atoms. The adsorption of the molecule produces also a significant displacement of the Cu surface atoms out from their equilibrium positions, resulting in a corrugation of the top Cu layer of 0.16 Å. In the case of the protonated molecule, the optimized configuration presents the carboxyl groups rotated with the oxygen in the OH group moving upwards by 0.35Å with respect to the C atom in the group, and the other O moving downward by 0.15Å. This means that even in the case of the protonated TPA

molecule there is a rather strong O-Cu bonding.

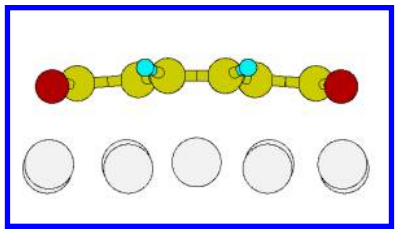

Figure 8: Side view of the lowest-energy adsorption geometry obtained for the (3×3) phase of TPA molecules on Cu(001).

Having studied the case of isolated molecules, the next step is to study the energetic and the properties of the (3×3) phase. In a 3×3 supercell there is no enough space for the molecule in the [110] orientation and therefore the molecular configuration must be the one shown in Fig. 1. In this superstructrure, the optimized adsorption geometry of the molecule is very similar to the isolated one, with a bending of 0.26 Å between the height of the benzene and the O atoms, and a corrugation in the last Cu layer of 0.16 Å(see Fig. 8). The calculated adsorption energy per molecule is of 2.28 eV, indicating a stabilization of the ordered phase with a gain of 0.20 eV per molecule. This energy gain has contributions from direct molecule interactions, mainly by formation of [C-H$\cdots$ O] bonds, and from substrate mediated interactions. As pointed out by Tseng *et al*,[4] the molecule-induced surface corrugation can cause an attractive intermolecular interaction.

From the relaxed structure of this (3×3) phase, we simulated STM images for positive and negative bias voltage V_b. Fig. 9 compares the simulated images obtained for $V_b = \pm 1.6$ V with the experimental ones taken at RT for the same bias voltages. In the experiment, the change of polarity produces an observable change in the shape of the molecular images. It can be seen that, while at -1.6 V the molecules appear as ellipsoids elongated along the [100] directions, at +1.6 V the molecular images are approximately circular. These experimental images are part of a wider study of the bias-voltage dependence of the molecular image which covered the range between -2 and +2 V. We found ellipsoidal shapes from -2 V to +0.5 V, approximately, while circular shape spots were clearly observed above +1.5 V. The simulated images shown in Fig. 9 reproduce the observed effect qualitatively. In the simulations, the molecules are imaged as spots with the brighter zone in

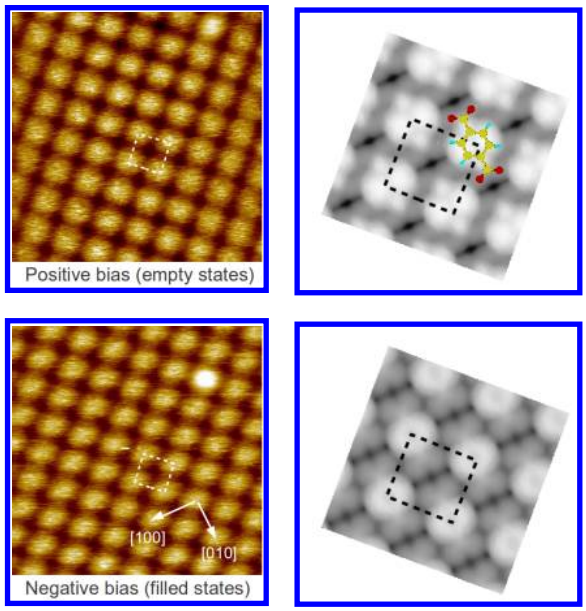

Figure 9: Experimental (left) and simulated (right) STM images of the (3×3) phase for positive and negative sample bias. Top: $+1.6$ V Bottom: -1.6 V. The tunneling current and the size values corresponding to the experimental images are 100pA and (70×70) Å^2, respectively. The unit cell is shown in each image as a dashed square. The molecule orientation is shown in the simulated positive-bias STM image.

the position of the C rings.

In order to understand the behavior of the STM images with the bias voltage, we analyzed the total and projected density of states (PDOS) of this phase. Fig. 10 shows the total DOS calculated for the relaxed structure of the phase in a region of ± 3 eV around the Fermi level and also the projections of the DOS on the benzene ring (atoms labeled C1 and C2), on the C atoms of the carboxyl groups (labeled C3) and on the oxygen atoms. The PDOS related to the benzene ring dominates the total density of states above the Fermi level. In particular, it is responsible of the two features at 0.0-0.7 eV and 1.8-3.2 eV. On the other hand, the DOS corresponding to the filled-states is dominated by the PDOS associated with the O atoms. The main features appears below 1 eV, where the Cu d band begins, and a clear hybridization with O orbitals can be seen in the figure. The relative small contribution of O p_z orbitals means that although the O atoms are close to a top position, the main hybridization comes from p_x and p_y orbitals pointing to the corresponding neighbor Cu atom. Although the O atoms have a high contribution for energies up to -1.6 eV,

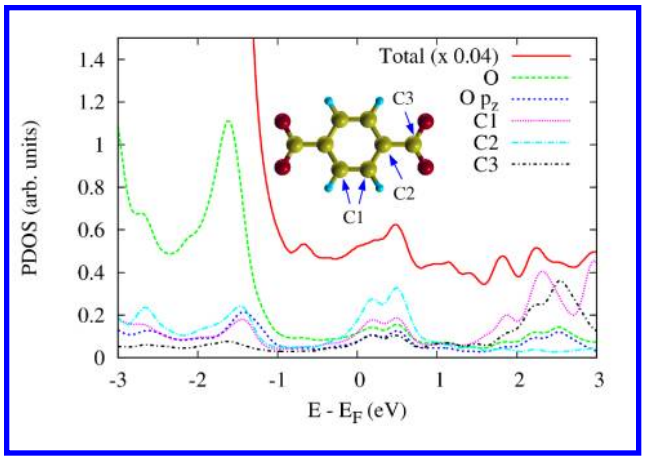

Figure 10: Calculated projected density of states (PDOS) corresponding to the (3×3) phase of deprotonated TPA molecules on the Cu(001) surface.

the difference in height with respect to the benzene ring (0.26 Å) make them less visible in the STM images. The change in the spots shape of the STM images for positive and negative bias, can be understood taking into account the difference in height between the C atoms in the ring ($z_{C1} - z_{C2} = 0.1$ Å) and their corresponding PDOS (Fig. 10). In fact, for negative bias both ring atoms have approximately the same PDOS, making the C2 atoms less visible in the STM image due to their lower height. On the other hand, for positive bias C2 atoms have a higher contribution in the PDOS, that compensate their lower height and became more visible, resulting in the square-like shape in the STM images.

Therefore, by comparing the experimental and simulated images, we can conclude that the spots in the negative bias STM images are elongated perpendicular to the long molecular axis.

For the molecular configuration in the $9\sqrt{2}$ phase, the high-resolution STM image shown in the upper part of Fig. 11, as well as the one in Fig. 4(b) of Stepanow *et al*,[12] suggest that the molecules are adsorbed with the long axis parallel to the [110] and [$\bar{1}$10] directions. Since our HR-XPS data indicate that this phase contains both complete and deprotonated carboxyl groups, we have performed DFT calculations for possible configurations with different degree of deprotonation. Moreover, we also considered the possible formation of structures with Cu adatoms, already observed by Wang *et al* for TPA adsorption on Cu(110).[37]

In Fig. 12 we show the four relaxed configurations which have the highest adsorption energy,

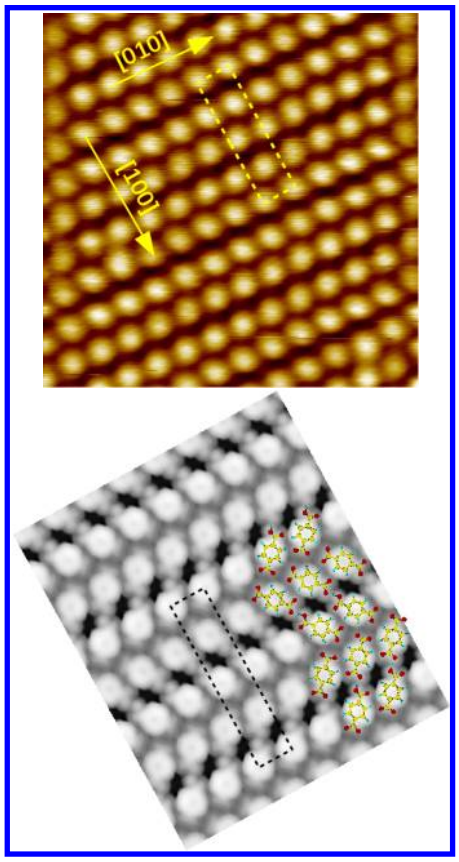

Figure 11: Experimental (top) and simulated (bottom) STM images for the $9\sqrt{2}$ phase. The unit cell is shown as dashed rectangles in both STM images. The tunneling conditions and the size corresponding to the experimental image are -2.0V/50pA and (100×100) Å^2, respectively.

out of eight considered configurations. The two calculated relaxed structures with adsorbed Cu atoms are not shown as they have lower molecule adsorption energy by more than 0.20 eV. In this figure, configuration (a) corresponds to semi-deprotonated molecules as proposed by Stepanow *et al*[12] but with a different arrangement of the OH groups of the molecules, configuration (b) corresponds to totally deprotonated molecules, while (c) and (d) correspond to structures with a half of the molecules totally deprotonated and the other half semi-deprotonated. Among the configurations analyzed, configuration (d) is the most stable one. This configuration has an adsorption energy of 2.01 eV per molecule which is lower than the values obtained for the deprotonated molecule, both isolated or in the (3×3) phase, but higher than the value obtained for the complete adsorbed molecule. From the rather large difference (> 0.20 eV) in the adsorption energy for this

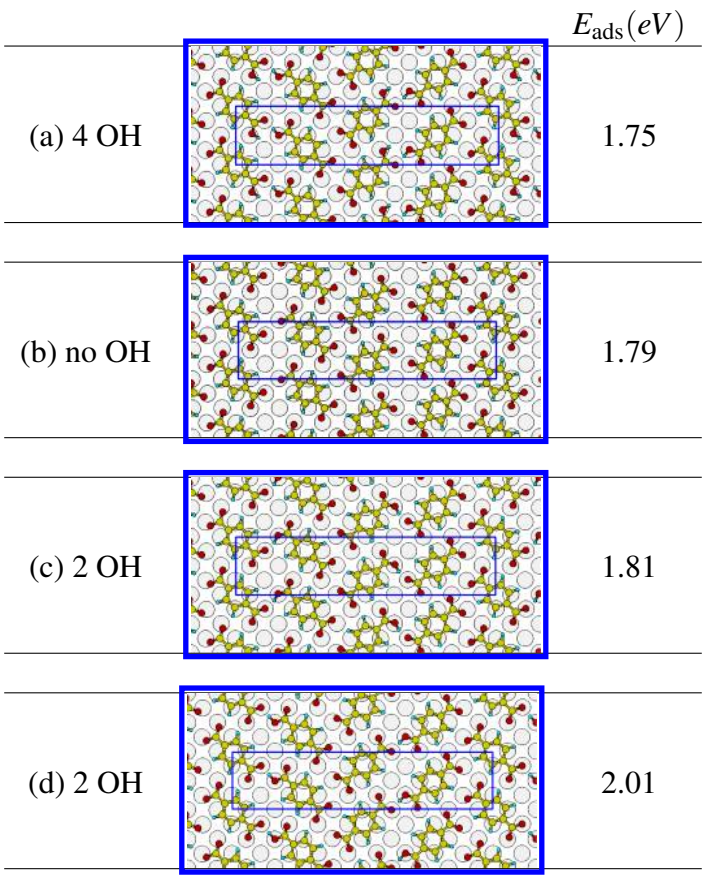

Figure 12: Relaxed configurations of different possible molecular geometries for the $9\sqrt{2}$ phase, which are close in adsorption energy. For each configuration, we indicate: on the left the number of OH groups, and on the right the corresponding adsorption energy per molecule in eV.

molecular geometry compared to the other possible configurations, we conclude that this is the molecular configuration of the $9\sqrt{2}$ phase.

As shown in detail in Fig. 13, the $9\sqrt{2}$ unit cell thus contains 2 RCOOH groups and 6 deprotonated groups (RCOO-), with the RCOOH groups facing the RCOO- ones. To simplify the analysis, we classify the 16 O atoms in four chemically-inequivalent groups, two of them coming from the RCOOH groups (denoted by O_{p1} and O_{p2}) and the other two coming from the deprotonated carboxyl ones (O_{d1} and O_{d2}). Although O_{d1} atoms belong to deprotonated groups, they form H-bonds and we then expect some difference with respect to the rest of O atoms in RCOO- groups (O_{d2} atoms). For the relaxed structure, we calculated the distances of the O atoms to the Cu nearest-neighbor, finding values of 2.08 Å, 2.23 Å, and 2.01-2.06 Å for the O_{p2}, O_{d1} and O_{d2}

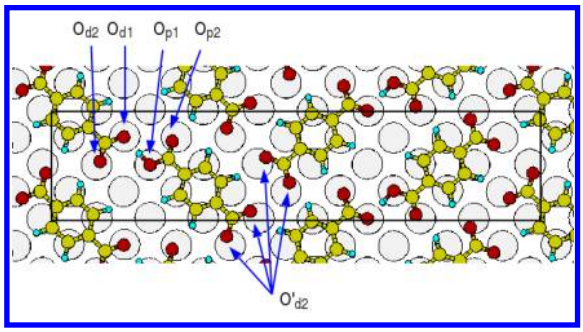

Figure 13: The $(9\sqrt{2} \times 2\sqrt{2})$R45° unit cell corresponding to the lowest-energy configuration. O_{p1} and O_{p2} are chemically-inequivalent O atoms coming from the complete carboxyl groups while, in turn, O_{d1}, O_{d2} and O'_{d2} are chemically-inequivalent O atoms coming from the carboxylates. See text for details.

atoms respectively. We can see that the O_{d1} atoms are displaced upwards significantly due to the formation of the hydrogen bond.

In order to further elucidate the contributions of the O_{p2} and O_{d1} atoms to the XPS O1s spectrum (Figure 6), we calculated the relative shifts of O1s levels of all O atoms in the unit cell. This relative core level shifts are calculated as total-energy differences of the same system containing a core hole at different positions.[40] In this way, the screening of the hole in the final state is taken into account. The core hole is described by means of a pseudopotential for O generated with a hole in the 1s level. Relative to the O_{p1} 1s level, we obtain values of 1.18 eV, 1.35 eV and 1.58-1.69 eV for the O_{p2}, O_{d1} and O_{d2} 1s levels respectively. We note that the shift higher than 0.2 eV between the core levels of the O_{d1} and O_{d2} atoms reflects the differences between the corresponding Cu-O bond lengths discussed above. In the inset of Figure 6, we show a simulated XPS spectrum using for each O peak a gaussian function with a width of 0.5 eV. It reproduces qualitatively well the experimental O 1s core level spectrum of the $9\sqrt{2}$ phase. Even when the calculated chemical shifts for the O_{p2} and O_{d2} 1s levels are systematically lower than the values expected for C=O and for carboxylate groups relative to OH peak, we can expect an experimentally-distinguishable shift of the O_{d1} peak with respect to the peak positions of the O_{d2} atoms. This effect might explain the shift of 1.6 eV and the higher intensity of component II with respect to component III.

Finally, from the relaxed structure of this configuration for the $9\sqrt{2}$ phase (Fig. 13), we sim-

ulated STM images for positive and negative bias voltage V_b. Fig. 11 compares the simulation obtained for $V_b = -2.0$ V with an experimental image taken at RT for the same bias voltages. In the simulated images the spots corresponding to the semi-deprotonated molecules are brighter than the spots of the totally deprotonated molecules. This difference comes from the OH groups which in the relaxed structure are higher from the surface than the C-ring. In the experimental images shown in Fig. 11, there is no appreciable difference in brightness between lines of spots. However, several other images present this effect as we show in Fig.14. This image presents a region where we clearly see alternate lines with brighter spots, and the abrupt change in the top of this region points to an effect due to the STM tip.

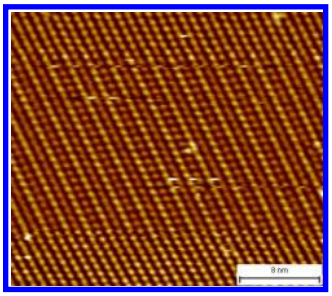

Figure 14: Experimental STM image of the $9\sqrt{2}$ phase taken with a bias voltage of -2 V and a tunneling current of 10 pA. This image illustrates how the appearance of the $9\sqrt{2}$ phase can change due to tip effects.

Discussion

We show in Fig. 15 a comparative scheme of the adsorption energy values obtained for the different phases analyzed theoretically in this work. The first column starting from the left shows the adsorption energies obtained for isolated molecules, the second one corresponds to the cases of the $9\sqrt{2}$ and the 3×3 phases, both of them corresponding to a molecular coverage of 1 molecule per 9 Cu atoms of the first surface layer ($\theta = 1/9$). In the third column we include a phase that was obtained from the calculations for a molecular coverage of 1 molecule per 8 Cu atoms of the first surface layer ($\theta = 1/8$). This phase corresponds to a $(2\sqrt{2} \times 4\sqrt{2})$R45° structure with two

deprotonated TPA molecules in the unit cell, oriented as in the $9\sqrt{2}$ phase but with a more compact arrangement, as can be seen in Fig. 16. Remarkably, the $c(3\times5)$ phase recently reported by Tait et al.[35] for the TPA/Cu(001) system most probably corresponds to the $(2\sqrt{2}\times4\sqrt{2})$R45° structure found in this work. In addition, a similar structure has also been recently observed for TPA molecules adsorbed on Cu(110).[37] Although with the $(2\sqrt{2}\times4\sqrt{2})$R45° structure there is no gain in adsorption energy with respect to isolated molecules, it corresponds to the lying down phase with the highest possible molecule coverage.

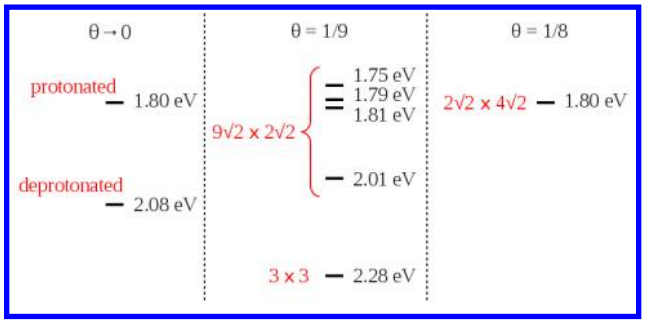

Figure 15: Summary of the adsorption energies theoretically obtained for the different phases and configurations considered in this work. Van-der-Waals interactions were considered in the corresponding DFT calculations. See text for details.

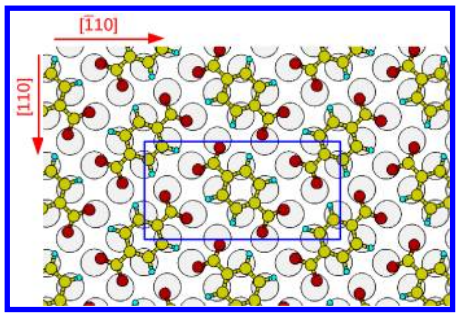

Figure 16: Molecular geometry for the calculated relaxed configuration of the $(2\sqrt{2}\times4\sqrt{2})$R45° molecular structure.

The 3×3 **phase.** As expected from the experimental data, the 3×3 phase is the most stable phase of the system, with an energy gain produced by the assembly of the phase of 0.20 eV per molecule (with respect to the isolated molecule). In this phase, the dominant molecule/substrate interaction comes from the formation of strong O-Cu bonds; it imposes a defined registry of the molecules with respect to the substrate. Specifically, the terephthalates are located with the center

of the C ring on a hollow site of the surface and the O atoms at positions nearly atop Cu atoms of the first surface layer; this adsorption geometry is very similar to that obtained for isolated deprotonated molecules. In addition, the formation of Cu-O bonds produces a bending of the molecules and a corrugation of the first Cu layer. Interestingly, the 6 C atoms of the rings are no longer equivalent as a consequence of the bending, producing an observable effect in the STM images.

Two main intermolecular interactions can then be identified as responsible of the self-assembly of the 3×3 phase: i) the formation of weak [C-H$\cdots$ O] hydrogen bonds between the O atoms of a molecule and the H atoms of the aromatic ring of its nearest-neighbor molecules and ii) surface-mediated interaction. Regarding the [C-H$\cdots$ O] bonds, a wealth of structural data revealed that the distance between H and O atoms, d(H$\cdots$ O), is typically found in the range [2.0-3.0] Å.[24] In the calculated 3×3 structure, the d(H$\cdots$ O) distance is 2.17 Å and the angle is 152.2°. We note that, while the distance is consistent with strong [C-H$\cdots$ O] bonds the angle is, in turn, quite far from the optimum one (180°).

On the other hand, it was recently shown that, in the case of 7,7 ,8,8-tetracyanoquinodimethane (TCNQ) adsorbed on Cu(001) surfaces, the buckling of the first substrate layer induced by the strong bonds formed between the cyano groups and the Cu atoms plays a determinant role in the molecular self-assembly.[4] It was shown that in this case the increase of the surface elastic energy produced by the buckling is the driving force for a strong surface-mediated attractive intermolecular interaction which leads to the molecular islanding. Our calculations for an isolated deprotonated TPA molecule (see figure 7) predict important vertical displacements ($\sim$0.12 Å) of the Cu atoms underneath the adsorbed molecule and, therefore, we can expect important surface-mediated intermolecular interactions also in the case of the 3×3 phase. As mentioned in the introduction section, Ge et al.[23] reported that no evidences of [C-H$\cdots$ O] bonds were detected in their HREELS spectra of the 3×3 phase and, hence, it was suggested that the TPA islanding may occur due to surface-mediated attractive interactions. Our theretical results are consistent with the proposed hypothesis.

The $9\sqrt{2}$ phase. This phase presents peculiar characteristics. It contains [O-H$\cdots$ O] bonds that are not formed between the two RCOOH groups but between an OH and an O atom of a deprotonated carboxyl group. Interestingly, our calculations predict that the O_{d1} atom (see figure 13) is displaced upwards due to the formation of the hydrogen bond, significantly reducing the interaction with the Cu atom beneath. In turn, O_{p2} atoms in the RCOOH groups get closer to their nearest-neighbor Cu atom achieving a bond distance close to that found in the relaxed 3×3 phase.

The obtained O-Cu distances for the relaxed structure reflect something that emerged from the theoretical analysis of the isolated molecules: despite the fact that the O_{p2} atoms belong to protonated carboxyl groups, the O_{p2}-Cu distance turned out to be practically the same as the O_{d2}-Cu one. Furthermore, they are close to the O-Cu distance (2.01 Å) obtained for the 3×3 phase.

The case of the O_{d1} atoms is specially interesting because, being part of carboxylates, they form [OH...O] bonds. The fact that the Cu-O distance (2.23 Å) is in this case considerably larger than that obtained for the O_{d2} atoms (2.01-2.06 Å), implies that the strength of the [O-H$\cdots$ O] interaction must be comparable to that of the Cu-O one. In general, our theoretical analysis predicts strong Cu-O bonds between the O atoms of carboxylates and the Cu atoms of the surface. This fact is clearly reflected in the case of isolated molecules, where two adsorption-energy minima were found for terephthalates corresponding to the two different orientations of the molecule; in both cases a considerable buckling of the first surface layer was obtained. Remarkably, the high strength of the [O-H$\cdots$ O] interaction is consistent with the fact that the values of the corresponding geometrical parameters practically coincide with those found in TPA crystals, i.e. they are close to ideal values. Specifically, the calculated distance between the O atoms of the [O-H$\cdots$ O] bonds in the $9\sqrt{2}$ structure is 2.57 Å while the calculated $\widehat{OHO}$ angle is 177.9°. On the other hand, the distance between O atoms in the TPA crystal was experimentally determined to be 2.61 Å.[41]

We note that, although the optimal orientation both for isolated molecules (by 0.20 eV) and for the 3×3 phase was determined to be the $< 100 >$ one, the four molecules in the $9\sqrt{2}$ unit cell are oriented along the $< 110 >$ and equivalent directions. We can then conclude that the formed [O-H$\cdots$ O] bonds are able to compensate the energy cost of a more expensive azimuthal orientation.

The network of [O-H$\cdots$ O] bonds thus play an essential role in the stabilization of the $9\sqrt{2}$ phase.

Finally, the strong interaction between the O atoms in carboxylates and the Cu atoms in the steps produces the reorientation of the steps along the $< 100 >$ directions. Notably, our STM images indicate that the molecules adsorb at the lower edge of the steps with their long axes oriented as in the $9\sqrt{2}$ phase, i.e. along $< 110 >$ directions. It is interesting to note that, although the adsorption of the molecules at RT produces an important mass transport in the surface, neither the 3×3 nor the $9\sqrt{2}$ phase contains Cu adatoms in their structures.

Conclusions

The main conclusions derived from this study are the following. Our theoretical results indicate the formation of strong bonds between the O atoms in carboxylates and the Cu atoms of the surface, which causes a bending of the molecules and a buckling of the first Cu layer. In the 3×3 phases, it was shown that the bending produces observable effects in the molecular STM images. It was also observed that the strong interaction between the carboxylates and the Cu atoms at the step edges causes the reorientation of the surface steps along the $< 100 >$ crystallographic directions.

Regarding the metastable β phase, it was experimentally determined that it has a $(9\sqrt{2} \times 2\sqrt{2})$R45° unit cell and exactly the same molecular coverage as the 3×3 phase (1 TPA molecule per 9 Cu atoms in the first surface layer). When TPA molecules are deposited on the Cu(001) sample kept at RT, most of them adopt the $9\sqrt{2} \times 2\sqrt{2})$R45° structure; this situation was found to be stable during several hours. The lowest-energy structure theoretically found for the $(9\sqrt{2} \times 2\sqrt{2})$R45° phase contains two totally deprotonated molecules and two semideprotonated molecules in the unit cell (see Fig. 13). In this molecular structure the [O-H$\cdots$ O] bonds are formed between an OH group and an O atom of a deprotonated carboxyl group. This network of [O-H$\cdots$ O] bonds plays a fundamental role in the stabilization of the structure.

With respect to the irreversible $9\sqrt{2} \rightarrow 3 \times 3$ transition, the results reported in this work conclusively show that it involves the following two processes: i) deprotonation of the neutral carboxyl

groups remaining in the metastable phase and ii) re-arrangement of the molecules into the 3×3 configuration.

Acknowledgments

We thank Dr. Magalí Lingenfelder for helpful discussions. We acknowledge financial support by the following Argentine institutions: CONICET (PIP 112 200801 00958), J.A. Balseiro and ANTORCHAS foundations, and ANPCYT (PICT2005/33432, PME 2003/118), UNCuyo(Grants 06/C390). We also acknowledge financial support from the ICTP-ELETTRA USERS PROGRAMME. We also thanks CONICET for the fellowships of N.M.-Q. and L.C. Three of us, J.D.F., J.E.G. and H.A. are members of CONICET of Argentina.

References

(1) Barth, J. V.; Costantini, G.; Kern, K. *Nature* **2005**, *437*, 671–679.

(2) Barth, J. V. *Annual Review of Physical Chemistry* **2007**, *58*, 375–497.

(3) Elemans, J. A. A. W.; Lei, S.; de Feyter, S. *Angew. Chem. Int. Ed.* **2009**, *48*, 7298–7332.

(4) Tseng, T.-C.; Urban, C.; Wang, Y.; Otero, R.; Tait, S. L.; Alcamí, M.; Écija, D.; Trelka, M.; Gallego, J. M.; Lin, N.; et.al., *Nature Chemistry* **2010**, *2*, 374–379.

(5) Stepanow, S.; Ohmann, R.; Leroy, F.; Lin, N.; Strunskus, T.; Wo, C.; Kern, K. *ACS Nano* **2010**, *4*, 1813–1820.

(6) Clair, S.; Pons, S.; Seitsonen, A. P.; Brune, H.; Kern, K.; Barth, J. *J. Phys. Chem. B* **2004**, *108*, 14585–14590.

(7) Cheng, Y. Y.; Sun, W.; Wang, Y.; Shao, X.; Xu, X.; Cheng, F.; Li, J.; Wu, K. *J. Phys. Chem. C Lett.* **2007**, *111*, 10138–10141.

(8) Zhou, H.; Dang, H.; Yi, J.-H.; Nanci, A.; Rochefort, A.; Wuest, J. D. *J. Am. Chem. Soc.* **2007**, *129*, 13774–13775.

(9) Dubois, L.; Zegarski, B.; Nuzzo, R. *Langmuir* **1986**, *2*, 412–417.

(10) Chen, Q.; Perry, C. C.; Frederick, B. G.; Murray, P. W.; Haq, S.; Richardson, N. V. *Surface Science* **2000**, *446*, 63–75.

(11) Messina, P.; Dimitriev, A.; Lin, N.; Spillmann, H.; Abel, M.; Barth, J. V.; Kern, K. *J. Am. Chem. Soc.* **2002**, *124*, 14000–14001.

(12) Stepanow, S.; Strunskus, T.; Lingenfelder, M.; Dmitriev, A.; Spillmann, H.; Lin, N.; Barth, J.; Wöll, C.; Kern, K. *J. Phys. Chem. B* **2004**, *108*, 19392–19397.

(13) Classen, T.; Lingenfelder, M.; Wang, Y.; Chopra, R.; Virojanadara, C.; Starke, U.; Contantini, G.; Fratesi, G.; Fabris, S.; de Gironcoli S.,; et.al., *J. Phys. Chem. A* **2007**, *111*, 12589–12603.

(14) Faraggi, M.; Rogero, C.; Arnau, A.; Trelka, M.; Ecija, D.; Isvoranu, C.; Schnadt, J.; Mart-Gastaldo, C.; Coronado, E.; Gallego, J.; et.al., *J. Phys. Chem. C* **2011**, *115*, 21177–21182.

(15) Parker, B.; Immaraporn, B.; Gellman, A. J. *Langmuir* **2001**, *17*, 6638–6646.

(16) Schnadt, J.; Rauls, E.; Xu, W.; Vang, R.; Knudsen, J.; Lægsgaard, E.; Li, Z.; Hammer, B.; Besenbacher, F. *Phys. Rev. Lett.* **2008**, *100*.

(17) Spillmann, H.; Dmitriev, A.; Nian, L. N.; Messina, P.; Barth, J. V.; Kern, K. *J. Am. Chem. Soc.* **2003**, *125*, 10725–10728.

(18) Lingenfelder, M.; Spillmann, H.; Dmitriev, A.; Stepanow, S.; Lin, N.; Barth, J. V.; Kern, K. *Chem. Eur. J.* **2004**, *10*, 1913–1919.

(19) Tait, S.; Wang, Y.; Costantini, G.; Lin, N.; Baraldi, A.; Esch, F.; Petaccia, L.; Lizzit, S.; Kern, K. *J. Am. Chem. Soc.* **2008**, *130*, 2108–2110.

(20) Wang, Y.; Fabris, S.; Costantini, G.; Kern, K. *J. Phys. Chem. C* **2010**, *114*, 13020–13020.

(21) Gambardella, P.; Stepanow, S.; Dmitriev, A.; Honolka, J.; de Groot, F. M. F.; Lingenfelder, M.; Gupta, S.; Sarma, D. D.; Bencok, P.; Stanescu, S.; et.al., *Nature Materials* **2009**, *8*, 189–193.

(22) Tseng, T.-C.; Lin, C.; Shi, X.; Tait, S. L.; Liu, X.; Starke, U.; Lin, N.; Zhang, R.; Minot, C.; Hove, M. A. V.; et.al., *Phys. Rev. B* **2009**, *80*, 155458.

(23) Ge, Y.; Adler, H.; Theertham, A.; Kesmodel, L. L.; Tait, S. L. *Langmuir* **2010**, *26*, 16325–16329.

(24) Desiraju, G. R. *Acc. Chem. Res.* **1996**, *29*, 441–449.

(25) Gotter, R.; Ruocco, A.; Morgante, A.; Cvetko, D.; Floreano, L.; Tommasini, F.; Stefani, G. *Nucl. Instrum. Methods Phys. Res. A* **2001**, *467*, 1468–1472.

(26) Floreano, L.; Naletto, G.; Cvetko, D.; Gotter, R.; Malvezzi, M.; Marassi, L.; Morgante, A.; Santaniello, A.; Verdini, A.; Tommasini, F.; et.al., *Rev. Sci. Instrum.* **1999**, *70*, 3855–3865.

(27) Cautero, G.; Sergo, R.; Stebel, L.; Lacovig, P.; Pittana, P.; Pedronzani, M.; Carrato, S. *Nucl. Instrum. Methods Phys. Res. A* **2008**, *595*, 447–459.

(28) Giannozzi, P.; Baroni, S.; Bonini, N.; Calandra, M.; Car, R.; Cavazzoni, C.; Ceresoli, D.; Chiarotti, G. L.; Cococcioni, M.; Dabo, I.; et.al., *J. Phys.: Condens. Matter* **2009**, *21*, 395502.

(29) Lee, K.; Murray, É. D.; Kong, L.; Lundqvist, B. I.; ; Langreth, D. C. *Phys. Rev. B* **2010**, *82*, 081101.

(30) Cooper, V. R. *Phys. Rev. B* **2010**, *81*, 161104.

(31) Bengtsson, L. *Phys. Rev. B* **1999**, *59*, 12301–12304.

(32) Tersoff, J.; Hamann, D. R. *Phys. Rev. B* **1985**, *31*, 805–813.

(33) We used the LEEDpat 3.0 software by K. Hermann and M.A. Van Hove.

(34) Katayama, T.; Mukai, K.; Yoshimoto, S.; Yoshinobu, J. *Phys. Rev. B* **2011**, *83*, 153403.

(35) Tait, S.; Lim, H.; Theertham, A.; Seidel, P. *Phys. Chem. Chem. Phys.* **2012**, *14*, 8217–8223.

(36) Giessen-Seibert, M.; Jentjens, R.; Poensgen, M.; Ibach, H. *Phys. Rev. Lett.* **1993**, *71*, 3521–3524.

(37) Wang, Y.; Fabris, S.; White, T.; Pagliuca, F.; Moras, P.; Topwal, M. P. D.; Sheverdyaeva, P.; Carbone, C.; Lingenfelder, M.; Classen, T.; et.al., *Chem. Commun.* **2012**, *48*, 534–536.

(38) McQuaide, B. H.; Banna, M. S. *Can. J. Chem.* **1988**, *66*, 1919–1922.

(39) Cossaro, A.; Puppin, M.; Cvetko, D.; Kladnik, G.; Verdini, A.; Coreno, M.; de Simone, M.; Floreano, L.; Morgante, A. *J. Phys. Chem. Lett.* **2011**, *2*, 3124–3129.

(40) Pehlke, E.; Scheffler, M. *Physical Review Letters* **1993**, *71*, 2338–2341.

(41) Bailey, M.; Brown, C. J. *Acta Cryst.* **1967**, *22*, 387–391.